Article

Ultra-Low Interfacial Tension Foam System for Enhanced Oil Recovery

Qi Liu [1],[†]**, Shuangxing Liu** [1],[†] **, Dan Luo** [2],* **and Bo Peng** [1],*

[1] Beijing Key Laboratory for Greenhouse Gas Storage and CO2-EOR, The Unconventional Petroleum Research Institute, China University of Petroleum (Beijing), Beijing 102249, China; liuqi@cup.edu.cn (Q.L.); shuangxing_liu@outlook.com (S.L.)

[2] State Key Laboratory of Heavy Oil Processing, College of New Energy and Materials, Beijing Key Laboratory of Biogas Upgrading Utilization, China University of Petroleum (Beijing), Beijing 102249, China

* Correspondence: luodan@iccas.ac.cn (D.L.); pengeor_cup@163.com (B.P.); Tel.: +86-1089-731-160 (D.L.); +86-1368-136-3093 (B.P.)

† These authors contributed equally to this work.

check for updates

Abstract: The liquid phase of foam systems plays a major role in improving the fluidity of oil, by reducing oil viscosity and stripping oil from rock surfaces during foam-flooding processes. Improving the oil displacement capacity of the foam's liquid phase could lead to significant improvement in foam-flooding effects. Oil-liquid interfacial tension (IFT) is an important indicator of the oil displacement capacity of a liquid. In this study, several surfactants were used as foaming agents, and polymers were used as foam stabilizers. Foaming was induced using a Waring blender stirring method. Foam with an oil-liquid IFT of less than 10–3 mN/m was prepared after a series of adjustments to the liquid composition. This study verified the possibility of a foam system with both an ultra-low oil-liquid IFT and high foaming properties. Our results provide insight into a means of optimizing foam fluids for enhanced oil recovery.

Keywords: Foaming method; foam system; liquid composition; ultra-low oil–liquid interfacial tension

1. Introduction

Compared to conventional liquids, foam fluid has several unique properties, such as, a high apparent viscosity, a high system energy, and a blocking effect. Foam fluid has been utilized in oil recovery as a tertiary oil recovery technology [1,2]. Foam flooding has been well studied for several decades and has been used in oil recovery worldwide [3]. The properties of foam fluids related to oil recovery can be modified to better adapt to the geological conditions; this is usually accomplished by changing the composition, preparation method, and/or preparation conditions of the foam system [4,5]. Most improvements have focused on improving the stability, salt resistance, temperature resistance and oil resistance of the foam [6,7]. Bubbles in the foam fluid can lose their shape over the course of the flooding process, as the foam system is in a state of foaming-flowing-defoaming dynamic equilibrium in the porous media encountered. Thus, all components of the foam system (the liquid, gas, and bubbles) play an important role in the flooding process [8,9].

Studies have shown that the interfacial tension (IFT) of the displacement phase strongly influences flooding effects [10,11]. A low IFT system refers to a system with an IFT between 10^{-2} and 1 mN/m; in ultra-low IFT systems, the IFT is below 10^{-2} mN/m. A low IFT system is better able to strip crude oil from rock surfaces by improving the fluidity of the crude oil [12,13]. Therefore, reducing the IFT of the displacement phase is an effective method to improve the flooding effect [14]. In addition, stability is an important indicator of the foam's performance [15,16]; an ideal foam system maintains high stability while adjustments are made to its IFT.

In this study, several surfactants [hexadecyl trimethyl ammonium bromide (CTAB), sodium oleate (SO), sodium dodecyl sulfate (SDS) and dodecyl hydroxypropyl phosphate betaine (DHPB)] and polymers [anion- polyacrylamide (APAM) and xanthan gum (XC)] were selected as additives, and dehydrated crude oil and simulated formation water representing that from the Dagang Oilfield were also used in this study. A foam system with an ultralow IFT liquid phase was generated by changing the chemical composition of the foam and the stirring method. To further investigate the foam's stability, a 1000 mL measuring cylinder was used to test the foaming capacity. This study systematically investigated the effect of surfactants on the stability and oil-liquid IFT of the foam, to gain insight into the means to improve foam flooding applications for enhanced oil recovery (EOR).

2. Materials and Methods

2.1. Liquid

The liquid used in this study simulated the mineral composition of true water in the Dagang Oilfield, which consists of deionized water and inorganic salts. The formation water was of the NaCl-KCl type; its ion composition is shown in Table 1. The inorganic salts used in this study are shown in Table 2.

Table 1. Ion composition of the Dagang Oilfield.

Ion	$Na^+ + K^+$	Ca^{2+}	Mg^{2+}	HCO_3^-	SO_4^{2-}	Cl^-	CO_3^{2-}	Salinity
concentration (mg/L)	4459	356	116	966	539	2989	437	9862

Table 2. Inorganic salts used in this study (AR, refers to Analytical Reagent).

| Inorganic Salt	Purity	Manufacturer
NaCl	AR	Macklin
KCl	AR	Macklin
$CaCl_2 \cdot 2H_2O$	AR	Macklin
$MgCl_2 \cdot 6H_2O$	AR	Macklin
Na_2CO_3	AR	Macklin
Na_2SO_4	AR	Macklin
$NaHCO_3$	AR	Macklin

2.2. Additives

Based on previous research [17–19], ten surfactants and four polymers were selected as foaming agents and stabilizers, respectively. Details of the additives are listed in Table 3, the molecular structure of the surfactants are shown in Figure 1. All chemicals were produced by Macklin (Shanghai Macklin Biochemical, Ltd., Shanghai, China). The critical micelle concentration (CMC) of each surfactant was tested using a conductivity method. The viscosity of each polymer was obtained using a viscometer.

Table 3. Chemicals used in this study.

Chemical	Purity	Type	Critical Micelle Concentration (CMC) at 25 °C
Tetradecyl hydroxypropyl phosphate betaine (THPB)	40%	Amphoteric	1200 mg/L
Dodecyl hydroxypropyl phosphate betaine (DHPB)	45%	Amphoteric	1360 mg/L
3-sulfopropyltetradecyl dimethyl betaine (3-SDB)	98%	Amphoteric	1000 mg/L
Cetyltrimethylammonium bromide (CTAB)	99%	Cationic	343 mg/L
Fatty amine polyoxyethylene ether (AC, C14)	99%	Nonionic	97 mg/L
α-Sodium olefin sulfonate (AOS, C12)	92%	Anionic	1932 mg/L
Sodium sulfate (SO)	96%	Anionic	365 mg/L
Sodium lauryl sulfate (AES)	70%	Anionic	2177 mg/L
Sodium dodecyl sulfate (SDS)	96%	Anionic	2307 mg/L
sodium dodecyl benzene sulfonate (SDBS)	99%	Anionic	418 mg/L
Chemical	**Purity**	**Type**	**Viscosity at 45 °C, 1 g/L**
Anionic polyacrylamide (APAM, 5 million molecular weight)	99%	Polymer	3331 mPa·s
Xanthan gum (XC)	USP	Polymer	9472 mPa·s
Nonionic polyacrylamide (PAM, 5 million molecular weight)	99%	Polymer	3922 mPa·s
Polysorbate 80 (Tween 80)	40%	Polymer	493 mPa·s
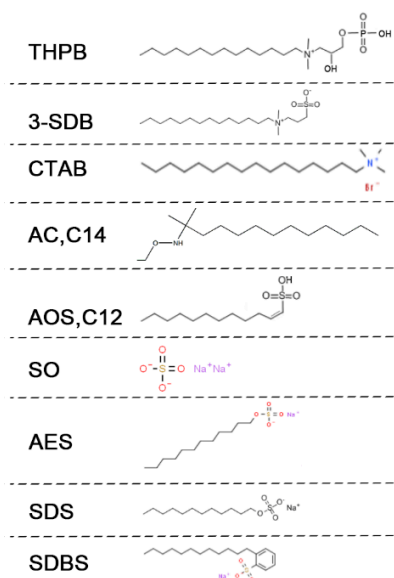
Figure 1. Molecular structure of the surfactants.

2.3. Foaming Process

Samples were composed of simulated formation water that contained a surfactant and a polymer. To fully disperse the additives and mix the two phases (gas and liquid), a Waring blender [20] (model 8010s, Waring Commercial, Connecticut, United States) was used. The gas (air) and liquid (solutions of surfactants (and polymers)) were stirred in the blender at 7000 revolutions (rev)/min for 3 min at 25 °C and 1 atm. Next, the foam was transferred into a measuring cylinder (1000 mL) to evaluate its foaming properties.

The stirring method applied to generate foams with minor modifications consisted of three steps: (i) preparing the surfactant-polymer solution; (ii) stirring the solution in the blender at a 7000 rev/min rotating speed for 3 min in a closed environment, air was used as gas phase; and (iii) moving the foam to the measuring cylinder.

2.4. Foaming Capacity and Foam Stability

The foaming volumes and residual-liquid volumes were measured by using scale markings of the Waring blender container. The half-life period was measured using the 1000 mL cylinder and

a stopwatch at 25 °C and 1 atm. The foam composite index (FCI) [21,22] was used as an indicator of the foam's comprehensive performance (foaming capacity and foam stability), according to the following equation:

$$\text{FCI} = \frac{3}{4} V_0 \cdot t_{\frac{1}{2}} \tag{1}$$

where: V_0 is the foaming volume (mL units) and $t_{1/2}$ is the foam half-life in minutes.

Table 4 shows the parameters that characterize foaming capacity and foam stability.

Table 4. Parameters of foaming properties used in this study.

Parameter	Symbol	Definition	Unit
Foaming volume	V_0	Volume of foam after foaming	mL
Residual-liquid volume	V_t	Volume of liquid remaining after foaming	mL
Foam half-life	$t_{1/2}$	Time required for the foam's volume to be reduced by half of its initial volume	min
Drainage half-life	t_D	Time required for the foam to lose half of its liquid	s
Foam composite index	FCI	Function of foaming volume and foam half-life	mL·min

2.5. Oil-Liquid IFT of Liquid Phase

Dehydrated crude oil from the Dagang Oilfield was selected as the research model. A rotary drop interface tension meter (SDT-500D, Harke, Beijing, China) was used to test the IFT between crude oil and the liquid. Sample measurements were performed three times, and the results were averaged.

2.6. Core-Flooding Experiment

Macroscopic flow characteristics of foam fluid in porous media and the EOR effect of the optimized foam system were investigated by a core-flooding experiment. The parameters of the artificial cores are shown in Table 5, the grouping of the core-flooding experiment is listed in Table 6, the experimental flow chart is shown in Figure 2.

Table 5. Parameters of the artificial cores used in the core flooding experiment.

Number	Water Permeability (mD)	Porosity (%)	Pore Volume (mL)
1	109	23.5	6.920
2	111	23.2	6.832
3	110	23.7	6.979
4	1.2	25.7	7.568
5	1	25.9	7.627
6	1	26.1	7.686

The core was cylindrical, and the size were 6 cm (length) × 2.5 cm (diameter), the volume was 29.45 cm^3. Numbers 1–3 were the high permeability group (≈110 mD), numbers 4–6 were the low permeability group (≈1 mD).

Table 6. Grouping of the core-flooding experiment.

Number	Group	Compounding	Core
1	Normal foam system	1.5 g/L SDS + 2 g/L PAM	NO.1
2	ASP	1 g/L SDBS + 6 g/L Na$_2$CO$_3$ + 1 g/L PAM	NO.2
3	Target foam system	1.2 g/L DHPB + 1.8 g/L SDS + 0.075 g/L XC	NO.3
4	Normal foam system	1.5 g/L SDS + 2 g/L PAM	NO.4
5	ASP	1 g/L SDBS + 6 g/L Na$_2$CO$_3$ + 1 g/L PAM	NO.5
6	Target foam system	1.2 g/L DHPB + 1.8 g/L SDS + 0.075 g/L XC	NO.6

Two commonly used chemical flooding methods (i.e., normal foam flooding and alkali-surfactant-polymer (ASP) flooding) were selected as the control groups. All chemical flooding

processes were conducted after water flooding (water flooding was suspended when the water content of produced fluid was more than 98%).
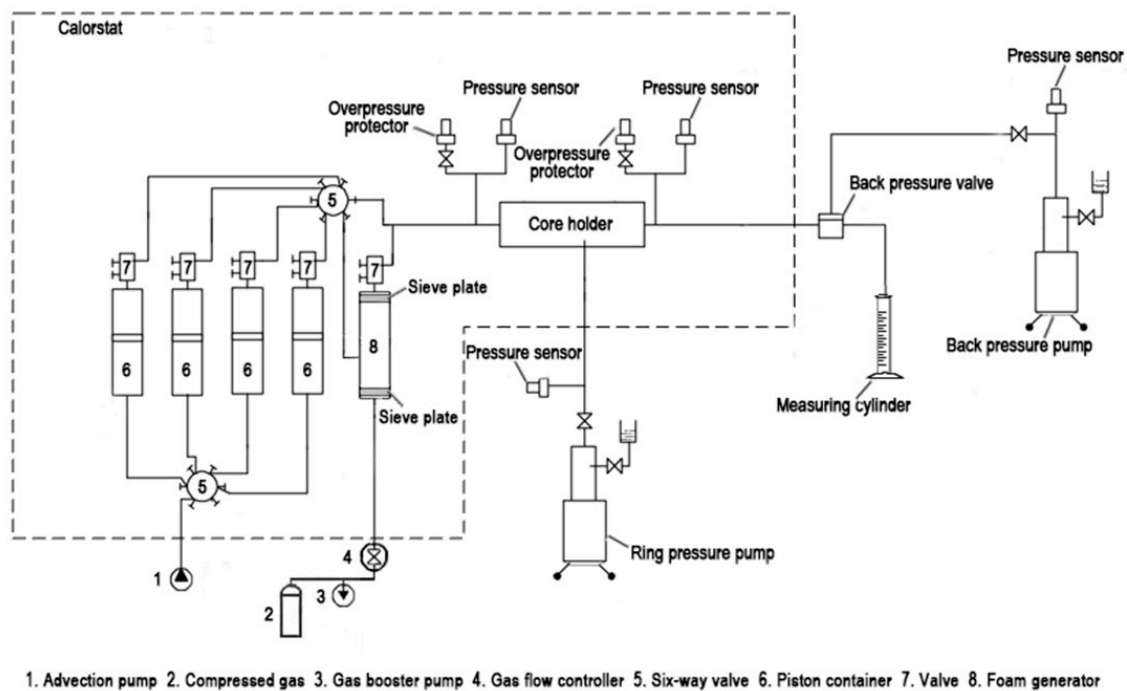

1. Advection pump 2. Compressed gas 3. Gas booster pump 4. Gas flow controller 5. Six-way valve 6. Piston container 7. Valve 8. Foam generator

Figure 2. Flow chart of core-flooding experiment.

A foam generator was used in this section for the foaming process. The foam generator had a set of sieve plates (three layers, 200 mesh, 2 mm spacing) at both the inlet and outlet. N_2 was used as the gas phase of the foam systems. The temperature was maintained by calorstat at 85 °C, the pressure in the core holder was controlled by back pressure pump at 20 MPa.

The macroscopic flow characteristics were investigated by the differential pressures at both ends of the core during injection process. The EOR effect was measured by the recovery efficiency of chemical flooding (after water flooding).

3. Results and Discussion

3.1. Foaming Properties and Oil-Liquid IFT of Surfactants

To evaluate the foaming ability, foam stability, and IFT of a single surfactant foaming system, solutions of each surfactant (100 mL) of various concentrations (0.05, 0.1, and 0.15 g/L) were stirred at 7000 rev/min for 3 min to generate foam. The resulting foam properties and oil-liquid IFT reduction capabilities are listed in Table 7.

Table 7. Foaming properties and oil-liquid interfacial tension (IFT) of individual surfactants.

Surfactant	Concentration (g/L)	V_0 (mL)	V_t (mL)	$t_{1/2}$ (min)	t_D (s)	FCI (mL·min)	IFT (mN/m)
THPB	0.05	210	65	151	175	23,782.5	0.4068
	0.1	265	35	158	180	31,402.5	0.5533
	0.15	235	40	168	54	29,610	0.6883
DHPB	0.05	190	50	110	92	15,675	0.3245
	0.1	215	25	129	103	20,801	0.2834
	0.15	235	15	131	115	23,088	0.2214
3-SDB	0.05	155	65	110	57	12,787.5	0.8971
	0.1	200	50	127	52	19,050	0.7324
	0.15	185	50	176	67	24,420	0.6021
CTAB	0.05	190	45	60	35	8550	0.2914
	0.1	240	40	57	28	10,260	0.2429
	0.15	180	55	60	31	8100	0.3755
AN	0.05	140	60	120	33	12,600	0.8395
	0.1	130	65	96	30	9360	0.8524
	0.15	145	50	80	23	8700	0.9455
AOS	0.05	255	35	83	135	15,873.75	1.2123
	0.1	280	20	90	160	18,900	1.1084
	0.15	285	15	73	104	15,603.75	1.3633
SO	0.05			No bubble			0.0025
	0.1	35	95	140	84	3675	0.0016
	0.15	60	80	600	90	27,000	0.0038
AES	0.05	110	60	92	100	7590	2.3112
	0.1	265	25	78	129	15,502.5	2.2219
	0.15	260	30	90	133	17,550	2.3794
SDS	0.05	250	25	90	77	16,875	0.795
	0.1	260	25	108	70	21,060	0.792
	0.15	275	20	99	73	20,419	1.0666
SDBS	0.05	175	25	18	42	2362.5	0.7434
	0.1	220	20	19	43	3135	0.6241
	0.15	220	20	22	52	3630	0.6432

Among the anionic surfactants, SO showed weak foaming properties due to poor solubility. The cationic surfactant CTAB possessed strong foaming capacity but weak foam stability. SDS and AES showed both strong foaming capacity and good foam stabilization effects. Amphoteric surfactants (THPB, DHPB and 3-SDB) exhibited good foaming properties and a high FCI. As the hydrophobicity of the hydrophobic group increased, the surfactant molecules distributed themselves closer to the gas-liquid interface. Compared with other surfactants, THPB, DHPB, and CTAB exhibited stronger hydrophobicity due to their longer alkyl chain, resulting in better foaming capacity. The foam stability was dependent on the liquid viscosity and the compactness of surfactants' arrangement on the interfaces. Thus, the same surfactant exhibited better foam stability at high concentration.

Similar to the foaming properties, the oil-liquid IFT of the surfactant solution was mainly influenced by the strength of the hydrophilic chain. A stronger hydrophobic chain led to stronger bonding between surfactant molecules and water molecules, improving the ability of the surfactant to reduce the IFT. Therefore, solutions of the surfactants with stronger hydrophilic chains, including SO, CTAB and THPB, had a lower oil-liquid IFT.

3.2. Foaming Properties and Oil-Liquid IFT of Binary Surfactants

Corrosion and blockage can be caused by chemical reactions between cationic surfactants and the formation. Nonionic surfactants often have weak solubility. Therefore, anionic and amphoteric surfactants were used for compounding in this study. Based on the results shown in Table 7, THPB, DHPB, AOS, AES and SDS were selected for compounding. The compounding scheme and test results are shown in Table 8. The total concentration of each surfactant was 0.3 g/L.

Table 8. Foaming properties and oil-liquid IFT of compound systems.

Compound System	Mass Ratio	V_0 (mL)	V_t (mL)	$t_{1/2}$ (min)	t_D (s)	FCI (mL·min)	IFT (mN/m)
THPB:AOS	1.5:1	245	15	122	76	22,417.5	0.7145
	1:1	260	15	103	71	20,085	0.7982
	1:1.5	270	15	92	78	18,630	0.9054
THPB:AES	1.5:1	360	10	101	145	27,270	0.0154
	1:1	450	10	114	161	38,475	0.0134
	1:1.5	530	5	300	192	119,250	0.0107
THPB:SDS	1.5:1	310	15	76	78	17,670	0.0692
	1:1	330	15	91	78	22,522.5	0.0631
	1:1.5	370	10	102	81	28,305	0.0545
DHPB:AOS	1.5:1	95	35	47	43	3348.75	0.5789
	1:1	115	30	46	47	3967.5	0.6541
	1:1.5	145	30	57	47	6198.75	0.7763
DHPB:AES	1.5:1	80	45	18	36	1080	0.7316
	1:1	90	45	18	39	1215	0.7145
	1:1.5	115	40	21	37	1811.25	0.7682
DHPB:SDS	1.5:1	470	5	234	240	82,485	0.0089
	1:1	515	5	242	256	93,472.5	0.0084
	1:1.5	560	5	280	334	117,600	0.0076

The compound of DHPB and SDS (mass ratio: 1.5:1 to 1:1.5) had both an ultra-low oil-liquid IFT and high foaming properties (Table 8). A strong electrostatic attraction existed between the positive charge of the hydrophilic group of DHPB and the negative charge of the hydrophilic group of SDS [23]. This attraction impacted on the diffusion behavior of surfactant molecules at the interfaces and made foam generation easier. Meanwhile, electrostatic attraction facilitated the formation of a tight adsorption membrane at the interface, which led to higher foam stability and lower oil-liquid IFT.

According to the results shown in Table 8, the compounding of surfactants with the same carbon number showed a better synergistic effect. Because the carbon number of the surfactant molecule could affect the diffusion rate of the surfactant, the diffusion of surfactant molecules with the same carbon number may be more balanced, and the arrangement of the surfactant molecules on the interfaces more even. This ensures the adsorption of two surfactants on the interfaces and leads to two surfactants with similar diffusion rates. Thus, local IFT imbalance was minimized.

3.3. Foam Stabilizer Selection

Foam stabilizers (i.e., polymers) improve the stability of foam mainly by increasing the viscosity of the foam system's liquid phase [24,25]. Therefore, the concentration of the polymer solution may be an important indicator of its ability to stabilize the foam system. The viscosity-temperature curve (shear rate: 0.1 s^{-1}) and viscosity-shear rate curve (temperature at 45 °C) were obtained using a rheometer (Haake Mars III, Thermo Fisher Scientific, Waltham, MA, USA) to evaluate the effect of the stabilizers. The results are shown in Figure 3.
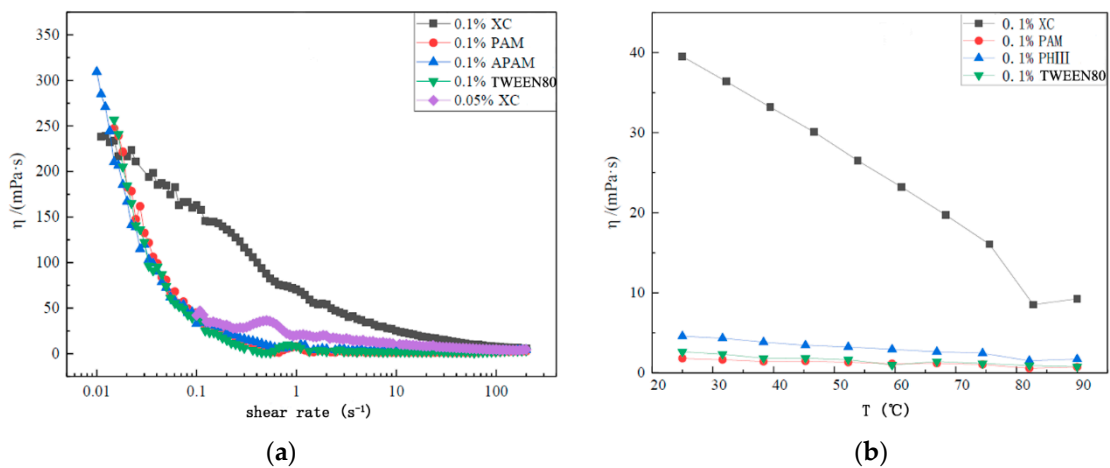
Figure 3. (**a**) Viscosity versus shear rate and (**b**) viscosity versus temperature.

The viscosity of XC at 0.1 g/L was higher than that of the other samples, given its shear rate of 0.03 s^{-1}, as shown in Figure 3a. Figure 3b shows that the viscosity of XC is higher than that of the other polymers over the temperature range of 20 °C to 90 °C. Common polymers are mostly linear structures, whereas XC has a double helix structure.

This double helix structure induces greater intermolecular entanglement and interaction between XC molecules; thus, the XC molecules maintain their structure better under external influences. In the presence of inorganic salts, XC molecules swell, which increases their viscosity. This feature ensures that XC performs better at high temperatures and under high salinity conditions.

3.4. Optimization of Foam System Performance

The surfactants (SDS at 0.18 g/L and DHPB at 0.12 g/L) were compounded with XC polymer, and the impact of the polymer's concentration on the oil-liquid IFT and foaming properties was investigated. Figure 4 shows the influence of the XC concentration on the oil-liquid IFT.
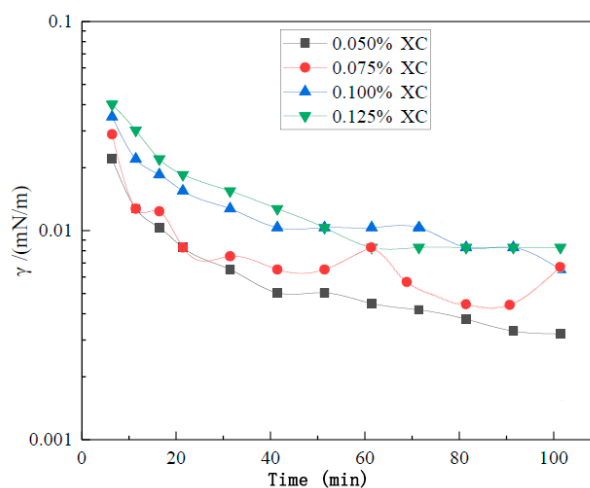

Figure 4. Influence of the xanthan gum (XC) concentration on oil-liquid interfacial tension.

The oil-liquid IFT increased with the XC concentration over time, as shown in Figure 4. Additionally, the adsorption rate of surfactant molecules from the liquid phase to the oil-liquid interface decreased as the XC concentration increased. However, the rate of the surfactant molecules' desorption from the oil-liquid interface to the oil phase did not change significantly, which eventually led to a decrease in the surfactant molecule concentration at the oil-liquid interface when the adsorption equilibrium was reached.

Table 9. Foaming properties varied with the XC concentration at different temperature.

Temperature (°C)	Concentration of XC (g/L)	V_0 (mL)	V_t (mL)	$t_{1/2}$ (min)	t_D (s)	FCI (mL·min)
25	0.05	535	5	278	631	111,547.5
	0.075	510	5	263	672	100,597.5
	0.1	460	0	242	714	83,490
	0.125	435	0	233	747	76,016.25
45	0.05	540	5	292	609	118,260
	0.075	525	0	281	681	110,643.75
	0.1	490	0	264	698	97,020
	0.125	450	0	247	704	83,362.5
65	0.05	495	15	231	519	85,758.75
	0.075	505	15	234	545	88,627.5
	0.1	455	10	209	571	71,321.25
	0.125	435	5	213	574	69,491.25
85	0.05	395	25	168	292	49,770
	0.075	420	25	184	341	57,960
	0.1	415	15	181	392	56,336.25
	0.125	405	15	190	403	57,712.5

With an increasing XC concentration, the foaming volume and the foam half-life of the system decreased slightly, but the drainage half-life of the foam increased significantly (Table 9). The foam viscosity increased with the XC concentration; thus, more energy was needed for the foaming process. However, the external energy obtained by the system stayed the same due to the same foaming method and stirring time, leading to a reduction in the foam volume. Meanwhile, the diffusion resistance of surfactant molecules increased with the liquid's viscosity. This resulted in localized thinning of the liquid film, a delay in the liquid film's self-repair, and a decline in the foam half-life. As the viscosity of the liquid increased, the liquid film's drainage rate and the gas diffusion rate decreased, which led to an increase in the drainage half-life.

Temperature could affect the stability of foam system by affecting viscosity, molecular motion, intermolecular force and molecular structure. According to the results in Table 9, the system with higher XC's concentration performed better foaming properties and foam stability at high temperature, and the system with lower XC's concentration had better performance at low temperature. This was mainly caused by the viscosity change [26], the viscosity of the system with high XC's concentration was too high at low temperature, but it could maintain a certain viscosity at high temperature. Therefore, it was concluded that the most suitable concentration of XC was 0.075 g/L based on the experimental results.

3.5. Macroscopic Flow Characteristics and EOR Effect

Figure 5 shows the differential pressure varied with the injection volume, and, the results of core-flooding experiment were shown in Table 10 (E_0 is the EOR rate of water flooding and E_c is the EOR rate of chemical flooding).
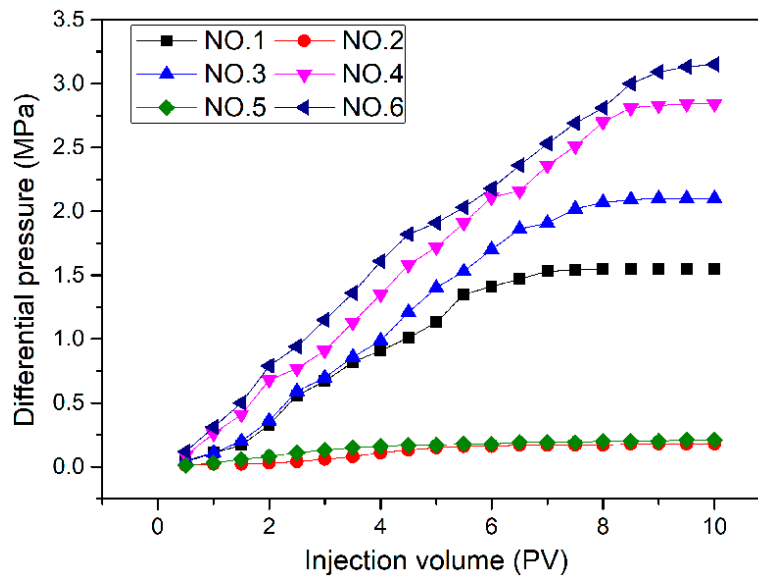
Figure 5. Differential pressure varied with the injection volume.

The foam flooding showed an obvious blocking effect, while the ASP flooding had almost no blocking effect. Meanwhile, the target foam system showed better blocking effect in both high permeability group (numbers 1–3) and low permeability group (numbers 4–6) than normal foam system. This results indicated that the Jamin Effect caused by the target foam system is more stable and effective than normal foam system. Which means, the target system could be more stable than normal foam system in porous media at high temperatures [27,28].

Table 10. Results of the core-flooding experiment.

Number	Oil Saturation (%)	E_0 (%)	E_c (%)
1	78.23	60.61	8.33
2	79.18	57.30	10.67
3	79.23	61.78	11.32
4	69.26	48.44	8.69
5	68.18	45.29	6.59
6	66.71	43.11	11.95

In high permeability group (numbers 1–3), the EOR rate of target foam flooding was nearly equivalent to ASP flooding, but significantly better than normal foam flooding. Commonly, blocking effect has a weak impact on the EOR rate in high permeability conditions [29], therefore, normal foam system performed a weak EOR effect. However, as the liquid phase had high EOR capacity (having ultra-low oil-liquid IFT), the target foam system showed better EOR rate than other two controlling group. In the low permeability group (numbers 4–6), the EOR effect of both foam flooding increased, but the ASP flooding's EOR effect declined sharply. In low permeability conditions, liquid with low viscosity could escape along the high permeability channels, thus, blocking effect could improve the EOR rate effectively [30,31].

4. Conclusions and Proposals

4.1. Conclusions

This study focused on strengthening the effect of a foam's liquid phase during the oil flooding process, in an attempt to prepare a foam system for EOR with high foaming properties and an ultra-low oil-liquid IFT. Several surfactants and polymers were evaluated. The foam composition was optimized

by adjusting the surfactant and polymer concentrations and combinations, with the goal of achieving a foam system with an ultra-low oil-liquid IFT and a high foaming capacity. The main conclusions are summarized below.

1. The foam system should have both a high foaming capacity and a low oil-liquid IFT obtained by using different surfactant and polymer structures and adjusting the composition of chemical additives.
2. The compounding of DHPB and SDS (mass ratio at 1:1.5) exhibited the best foaming properties (FCI: 117,600 mL·min) and the lowest oil-liquid IFT (0.0076 mN/m). The compounding of surfactants with the same carbon number showed better results.
3. Increasing polymer concentration lowered the oil-liquid IFT reduction rate, and led to an increase in the oil-liquid IFT. The viscosity of the liquid phase depends on the polymer concentration, which expected to affect the diffusion of surfactants and gas.
4. Ultra-low IFT foam system could function as both surfactant-polymer system and foam system in flooding process, which means it mainly functions in oil-liquid IFT reduction in high permeability conditions and blocks the high permeability channels in low permeability conditions. This feature meant the ultra-low IFT foam system could be more applicable in the EOR process.

4.2. Proposals

There have been few studies on the synergistic mechanisms of different surfactants. Investigations in this area are expected to provide a theoretical basis for subsequent research. Additionally, continued study of the effectiveness in EOR and migration in porous media of ultra-low IFT foam systems may provide new ideas for oil flooding and multiphase flow in porous media.

Author Contributions: Q.L. and S.L. performed the experiments, analyzed the data and wrote the paper; B.P. designed the experiments; D.L. and B.P. conducted the work and revised the paper.

Conflicts of Interest: The authors declare no conflict of interest.

References

1. Ahmed, S.; Elraies, K.A.; Tan, I.M.; Hashmet, M.R. Experimental investigation of associative polymer performance for CO_2, foam enhanced oil recovery. *J. Pet. Sci. Eng.* **2017**, *157*, 971–979. [CrossRef]
2. Talebian, S.H.; Masoudi, R.; Tan, I.M.; Zitha, P.L.J. Foam assisted CO2-EOR: A review of concept, challenges, and future prospects. *J. Pet. Sci. Eng.* **2014**, *120*, 202–215. [CrossRef]
3. Awan, A.R.; Teigland, R.; Kleppe, J. A Survey of North Sea Enhanced-Oil-Recovery Projects Initiated During the Years 1975 to 2005. *SPE Reserv. Eval. Eng.* **2008**, *11*, 497–512. [CrossRef]
4. Jones, S.A.; Van Der Bent, V.; Farajzadeh, R.; Rossen, W.R.; Vincent-Bonnieu, S. Surfactant screening for foam EOR: Correlation between bulk and core-flood experiments. *Colloids Surf. A Physicochem. Eng. Asp.* **2016**, *500*, 166–176. [CrossRef]
5. Guo, H.; Faber, M.J.; Buijse, M.A.; Zitha, P.L. A Novel Alkaline-Surfactant-Foam EOR Process. In Proceedings of the SPE Enhanced Oil Recovery Conference, Kuala Lumpur, Malaysia, 19–21 July 2011.
6. Ocampo, A.; Restrepo, A.; Cifuentes, H.; Hester, J.; Orozco, N.; Gil, C.; Castro, E.; Lopera, S.; Gonzalez, C. Successful Foam EOR Pilot in a Mature Volatile Oil Reservoir Under Miscible Gas Injection. *J. Pet. Technol.* **2013**, *65*, 117–119.
7. Druetta, P.; Raffa, P.; Picchioni, F. Plenty of Room at the Bottom: Nanotechnology as Solution to an Old Issue in Enhanced Oil Recovery. *Appl. Sci.* **2018**, *8*, 2596. [CrossRef]

8.   Talebian, S.H.; Masoudi, R.; Tan, I.M.; Zitha, P.L. Foam assisted CO_2-EOR; Concepts, Challenges and Applications. In Proceedings of the SPE Enhanced Oil Recovery Conference, Kuala Lumpur, Malaysia, 2–4 July 2013.

9.   Ahmed, S.; Elraies, K.A.; Tan, I.M.; Mumtaz, M. A Review on CO_2 Foam for Mobility Control: Enhanced Oil Recovery. In *ICIPEG 2016*; Springer: Singapore, 2017.

10. Srisuriyachai, F.; Pancharoen, M.; Laochamroonvoraponse, R.; Vathanapanich, Y. Reduction of Surfactant Adsorption: A Study of Dynamic Surfactant Adsorption/Desorption in Shaly-sandstone Reservoir. In Proceedings of the IOR 2019—20th European Symposium on Improved Oil Recovery, Pau, France, 8–11 May 2019.

11. Gu, Q.; Liu, H.; Zhang, Y. Lattice Boltzmann Simulation of Immiscible Two-Phase Displacement in Two-Dimensional Berea Sandstone. *Appl. Sci.* **2018**, *8*, 1497. [CrossRef]

12. Ologundudu, T.; Odiyo, J.; Ekosse, G.I. Fluoride Sorption Efficiency of Vermiculite Functionalised with Cationic Surfactant: Isotherm and Kinetics. *Appl. Sci.* **2016**, *6*, 277. [CrossRef]

13. Sahner, R.A.; Trivedi, K.; Puliafito, A. Generalized Correlations for Predicting Solubility, Swelling and Viscosity Behavior of CO2-Crude Oil Systems. *J. Petrol. Technol.* **1965**, *17*, 102–106.

14. Kang, P.S.; Lim, J.S.; Huh, C. Artificial Neural Network Model to Estimate the Viscosity of Polymer Solutions for Enhanced Oil Recovery. *Appl. Sci.* **2016**, *6*, 188. [CrossRef]

15. Yang, Y.; Gupta, M.C.; Dudley, K.L.; Lawrence, R.W. Conductive Carbon Nanofiber–Polymer Foam Structures. *Adv. Mater.* **2010**, *17*, 1999–2003. [CrossRef]

16. Holland, P.M.; Rubingh, D.N. Nonideal Multlcomponent Mixed Mlcelle Model. *J. Phys. Chem.* **1983**, *87*, 1984–1990. [CrossRef]

17. Hsu, Y.Y.; Gresser, J.D.; Trantolo, D.J.; Lyons, C.M.; Gangadharam, P.R.; Wise, D.L. Effect of polymer foam morphology and density on kinetics of in vitro controlled release of isoniazid from compressed foam matrices. *J. Biomed. Mater. Res. Part A* **1997**, *35*, 107–116. [CrossRef]

18. Farajzadeh, R.; Andrianov, A.; Zitha, P.L.J. Investigation of Immiscible and Miscible Foam for Enhancing Oil Recovery. *Ind. Eng. Chem. Res.* **2010**, *49*, 1910–1919. [CrossRef]

19. Tsujii, K.; Okahashi, K.; Takeuchi, T. Addition-compound formation between anionic and zwitter-ionic surfactants in water. *J. Phys. Chem.* **1982**, *86*, 1437–1441. [CrossRef]

20. Suh, K.W.; Krueger, D.C.; Zehner, B.E. Method for the Preparation of Styrene Polymer Foam. U.S. Patent NO. 4,438,224, 1986.

21. Zhou, S. Advances in Energy Science and Equipment Engineering II. *Eur. J. Nutr.* **2015**, *45*, 187–195.

22. Tang, S.; Tian, L.; Lu, J.; Wang, Z.; Xie, Y.; Yang, X.; Lei, X. A Novel Low Tension Foam Flooding for Improving Post-Chemical-Flood in Shuanghe Oilfield. In Proceedings of the SPE Improved Oil Recovery Symposium, Tulsa, OK, USA, 12–16 April 2014; Society of Petroleum Engineers: Richardson, TX, USA, 2014.

23. Rosen, M.J.; Hua, X.Y. Surface concentrations and molecular interactions in binary mixtures of surfactants. *J. Colloid Interface Sci.* **1982**, *86*, 164–172. [CrossRef]

24. Xiangchun, Z.; Junhui, Z.; Zhixue, S. Performance evaluation and study of flooding control of foam gel in SZ36-1 oilfield. *Petrochem. Ind. Appl.* **2012**, *41*, 57–59.

25. Willett, J.L.; Shogren, R.L. Processing and properties of extruded starch/polymer foams. *Polymer* **2002**, *43*, 5935–5947. [CrossRef]

26. Osterloh, W.T.; Jante, M.J. Effects of Gas and Liquid Velocity on Steady-State Foam Flow at High Temperature. In Proceedings of the SPE/DOE Enhanced Oil Recovery Symposium, Tulsa, OK, USA, 22–24 April 1992; p. 24179.

27. Martín, M.; García, J.M.; Montes, F.J.; Galán, M.A. On the effect of the orifice configuration on the coalescence of growing bubbles. *Chem. Eng. Process. Process Intensif.* **2008**, *47*, 1799–1809. [CrossRef]

28. Kamp, A.M.; Chesters, A.K.; Colin, C.; Fabre, J. Bubble coalescence in turbulent flows: A mechanistic model for turbulence-induced coalescence applied to microgravity bubbly pipe flow. *Int. J. Multiph. Flow* **2001**, *27*, 1363–1396. [CrossRef]

29. Liu, P.; Zhang, X.; Wu, Y.; Li, X. Enhanced oil recovery by air-foam flooding system in tight oil reservoirs: Study on the profile-controlling mechanisms. *J. Pet. Sci. Eng.* **2017**, *150*, 208–221. [CrossRef]

30. Chen, B.; Reynolds, A.C. Ensemble-based optimization of the water-alternating-gas-injection process. *SPE J.* **2016**, *2*, 11–20. [CrossRef]

31. Yu, J.; Mo, D.; Liu, N.; Lee, R. The application of nanoparticle-stabilized CO_2 foam for oil recovery. In Proceedings of the SPE International Symposium on Oilfield Chemistry, The Woodlands, TX, USA, 8–10 April 2013.